A.V. NESTEROV, M. SOLOKHA-KLYMCHAK

Bogolyubov Institute for Theoretical Physics, Nat. Acad. of Sci. of Ukraine
(14b, Metrolohichna Str., Kyiv 03680, Ukraine)

UDC 539

PROPERTIES OF $^{4}_{\Lambda}$H HYPERNUCLEUS IN THREE-CLUSTER MICROSCOPIC MODELS

Within the framework of microscopic three-cluster algebraic models with possible consideration of clustering types (D + n) + Λ, (D + Λ) + n, and (n + Λ) + D, the properties of discrete spectrum states of hypernucleus $^{4}_{\Lambda}H$ and continuous spectrum states in the $^{3}H + \Lambda$ channel are studied. It is shown that the cluster structure is almost completely determined by the clustering (D + n) + Λ with a rather appreciable effect from the polarization of the binary subsystem (D + n) due to its interaction with the Λ particle.

Keywords: cluster models, Resonating Group Method, three-cluster microscopic models, algebraic models, hypernucleus, cluster polarization.

1. Introduction

Nuclei containing, besides nucleons, also hyperons – i.e. strange baryons (they consist of u and d quarks, as well as one of the strange quarks) – are called hypernuclei. Hypernuclei – more specifically, Λ-hypernuclei – were experimentally discovered for the first time by M. Danysz and E. Pniewski, who, in 1953, among the products of nuclear fission by cosmic ray particles, revealed relatively long-lived fragments emitting pions.

A systematic experimental study of the properties of hypernuclei became possible after a meson beam had been created at CERN, which allowed hyperons to be created directly in atomic nuclei. For example, Λ-hypernuclei can be obtained by making use of the reactions

$$K^- + n \to \Lambda + \pi^-, \quad K^- + p \to \Lambda + \pi^0.$$

As a result, there arose a substantial interest in the study of the properties of hypernuclei, which has not faded for decades. Here, the main reason is that, along with nucleon systems, there appeared new systems of strongly interacting particles, which were available for study. This made it possible to obtain a new information about the strong interaction. The most promising is the study of the lightest hypernuclei, since they live much longer than the heavier ones, so more exact models can be used, while theoretically considering their properties.

From the total body of works, these are references to some of them: [1–10], which can help to get some idea of the current state of researches dealing with the properties of light hypernuclei and nucleon-hyperon interaction.

The object of our consideration is the hypernucleus $^{4}_{\Lambda}$H composed of a proton, two neutrons, and a Λ-hyperon. The latter, from the viewpoint of notions about the quark structure of hadrons, contains an u-quark, a d-quark, and an s-quark. The mass of Λ-hyperon is equal to 1115.68 MeV/c^2, its isospin is 0, spin 1/2, and lifetime 2.63×10^{-10} s. Owing to the weak interaction, the Λ-hyperon decays into a nucleon and a pion.

The hypernucleus $^{4}_{\Lambda}$H itself is nuclearly stable, i.e. it does not decay spontaneously with the emission of nucleons and a Λ-hyperon. It is known experimentally that $^{4}_{\Lambda}$H has two bound states with the total orbital angular momentum $L = 0$ at the positive parity, and the total angular momentum $J^\pi = 0^+$ or $J^\pi = 1^+$. The energies of those levels reckoned from the lowest threshold of the ^{3}H + Λ decay are equal to −2.04 and −1.05 MeV, respectively. The total binding energy of the nucleus is −10.52 MeV in the ground state and −9.53 MeV in the excited one. The lifetime equals 2.20×10^{-10} s. In the overwhelming majority of cases, the decay of $^{4}_{\Lambda}$H occurs through the ^{4}He + $+ \pi^-$ meson channel due to the weak interaction. The lifetime of $^{4}_{\Lambda}$H is somewhat shorter than the lifetime of free Λ-hyperon, which may be associated with a small admixture of meson-free decay channels of the type

$\Lambda + \mathrm{N} = \mathrm{N} + \mathrm{N}$, which are also a result of the weak interaction. For comparison, we note that the lifetime of ${}^{4}\mathrm{H}$ nucleus is approximately equal to 1.39×10^{-22} s, with ${}^{4}\mathrm{H} \to {}^{3}\mathrm{H}+\mathrm{n}$ being the main decay channel. The differences between the properties of ${}^{4}\mathrm{H}$ and ${}^{4}_{\Lambda}\mathrm{H}$ nuclei take place due to the fact that the ${}^{4}\mathrm{H}$ nucleus contains one proton and three neutrons, with one of them, in accordance with the Pauli principle, must be settled at least in the p-shell, whereas the Λ-hyperon and nucleons in the ${}^{4}_{\Lambda}\mathrm{H}$ hypernucleus can also be in the $(0s)$-state.

The models used in this work are presented in the next section. In Section 3, the input parameters of the problem are considered, and the results of numerical calculations are compared with available experimental data and theoretical results obtained by other authors.

2. Models Used to Consider the System Properties

The models used in this work to consider the system properties are three-cluster algebraic models based on the concept of the cluster structure of light atomic nuclei. Those concepts, in particular, form a basis of the Resonating Group Method (RGM) [11] and its algebraic version (AVRGM) [12,13]. The idea of the latter consists in that the function of the relative motion of the clusters is expanded in an oscillatory basis, which makes it possible to substantially simplify numerical calculations, because a significant part of calculations can be done analytically.

Our first model is actually nothing else than the three-cluster version of the AVRGM model. Below, it will be referred to as the Algebraic Model with the Oscillatory Basis (AMOB). In the other model, the function of the relative motion of a three-cluster system is expanded in both a binary Gaussian basis and a binary oscillatory one, which allows the bound states and all possible binary scattering channels of the third particle at binary subsystems to be considered with regard for the polarization of the latter. The Gaussian basis is very convenient when describing the bound states in both two- and multicluster systems, because it allows the convergence of results to be attained using a relatively small number of basis functions. The advantage of the oscillatory basis consists in that its application makes it possible to consider the boundary conditions both in discrete-spectrum and scattering problems simply and self-consistently. Below, this model will be referred to as the Algebraic Model with the Gaussian and Oscillatory Basis (AMGOB).

2.1. Algebraic model with the oscillatory basis (AMOB)

In accordance with the aforesaid, let us begin the presentation of our first model by writing down the total wave function of the system in the three-cluster case of the RGM,

$$\Psi = \hat{A}\left[\Psi_1\left(A_1\right)\,\Psi_2\left(A_2\right)\,\Psi_3\left(A_3\right)\Psi_{xy}\left(\mathbf{x},\mathbf{y}\right)\right], \qquad (1)$$

where $\hat{A}$ is an antisymmetrizer acting on the coordinates of identical particles, $\Psi_i\left(A_i\right)$ are preset functions that are given in the form of shell functions and describe the internal motion in the clusters, and $\Psi_{xy}\left(\mathbf{x},\mathbf{y}\right)$ is the function of the relative motion of the clusters. The latter, when solving the problem, is expanded in the basis of the functions of a six-dimensional harmonic oscillator, which are represented in hyperspherical variables. In the coordinate representation, those functions have the form

$$|n_\rho, K, l_x, l_y, LM\rangle = N_{n_\rho K}\exp\left\{-\frac{1}{2}\rho^2\right\}\rho^K \times$$
$$\times\, L^{K+2}_{K+2n_\rho}(\rho^2)\Phi_K^{l_x l_y LM}(\Omega). \qquad (2)$$

Here, n_ρ is the number of hyperradial excitation quanta, K is the hypermomentum, l_x and l_y are the partial angular momenta, L is the total angular momentum, M is its projection, ρ is the hyperradius. ($\rho^2 = \mathbf{x}^2 + \mathbf{y}^2$), and $\Phi_K^{l_x,l_y,L,M}(\Omega)$ is a hyperharmonic depending on five hyperangles. The relation between the magnitudes of the Jacobi vectors and the hyperradius is given by the formulas $x = \rho\sin\alpha$ and $y = \rho\cos\alpha$. The principal quantum number $N = K + 2n_\rho$.

It should also be noted that, for the fixed l_x- and l_y-values, the hypermomentum can take the values $K = l_x + l_y,\ l_x + l_y - 2,\ l_x + l_y - 4$, and so forth. This condition means that the sum of partial momenta does not exceed K. The partial angular momenta l_x and l_y determine the parity of the three-cluster state, namely, $\pi = (-1)^{l_x + l_y}$.

When considering the bound states and using an expansion of the wave function in the basis functions for the solution of the Schrödinger equation, we arrive at the following system of linear homogeneous

algebraic equations:

$$\sum_{\nu'}\Big[\langle\nu|\,\hat{H}\,|\nu'\rangle - E\,\langle\nu|\nu'\rangle\Big]C_{\nu'} = 0, \tag{3}$$

where, in our case, as follows from the above discussion, the composite index $\nu \equiv \{n_\rho, K, l_x, l_y, LM\}$; the set of coefficients $\{C_\nu\}$ represents the wave function of a system state in the oscillatory representation, and $\langle\nu|\,\hat{H}\,|\nu'\rangle$ and $\langle\nu|\nu'\rangle$ are the matrix elements of the Hamiltonian and the unit operator, respectively, calculated using the basis functions. An approach in which the K-harmonic basis is used was applied earlier with a certain success to describe the properties of bound states in three-cluster systems and the states of the continuous spectrum lying in the three-cluster continuum of borromean nuclei [14, 15].

2.2. Algebraic model with the Gaussian and oscillatory basis (AMGOB)

In this approach, the total wave function is represented in the form

$$\Psi^J = \hat{A}\left\{\left[\Phi_1(A_1)\,\Phi_2(A_2)\,\Phi_3(A_3)\right]_S \times \right.$$
$$\left. \times\left[f_1(\mathbf{x}_1,\mathbf{y}_1) + f_2(\mathbf{x}_2,\mathbf{y}_2) + f_3(\mathbf{x}_3,\mathbf{y}_3)\right]_L\right\}_J, \tag{4}$$

where $\hat{A}$ is the antisymmetrization operator acting on the variables of identical particles, $\Phi_\alpha(A_\alpha)$ is a shell function describing the internal motion in the α-th cluster ($\alpha = 1, 2, 3$), $f_\alpha(\mathbf{x}_\alpha, \mathbf{y}_\alpha)$ are the Faddeev components of the relative motion function, the Jacobi vector $\mathbf{x}_\alpha$ specifies the relative arrangement of the clusters β and γ, and the Jacobi vector $\mathbf{y}_\alpha$ connects the α-th cluster with the center of mass of the clusters β and γ.

Bipolar spherical harmonics are used for the Faddeev components,

$$f_\alpha(\mathbf{x}_\alpha,\mathbf{y}_\alpha) \Rightarrow f_\alpha^{(L)}(\mathbf{x}_\alpha,\mathbf{y}_\alpha) =$$
$$= \sum_{\lambda_\alpha, l_\alpha} f_\alpha^{(\lambda_\alpha, l_\alpha, L)}(\mathbf{x}_\alpha,\mathbf{y}_\alpha)\left\{Y_{\lambda_\alpha}(\hat{\mathbf{x}}_\alpha)\,Y_{l_\alpha}(\hat{\mathbf{y}}_\alpha)\right\}_{LM}, \tag{5}$$

which brings us to a set of four quantum numbers: $\lambda_\alpha, l_\alpha, L$, and M. The scheme of LS-bond is used, where the system spin $\mathbf{S}$, which is the vector sum of the spins of clusters, is linked to the orbital angular momentum $\mathbf{L}$ to form the total angular momentum $\mathbf{J}$. In the case of s-clusters, the total orbital angular momentum L is completely determined by the intercluster motion. The parity of three-cluster states is given by the formula $\pi = (-1)^{\lambda_\alpha + l_\alpha}$, where λ_α and l_α are the partial angular momenta.

We will use the expansion of the Faddeev components in both the oscillatory, $\{F_{n_\alpha l_\alpha m_\alpha}(\mathbf{y}_\alpha, b)\}$, and Gaussian, $\{G_{\lambda_{\mu\alpha}}(\mathbf{x}_\alpha b_{\nu_\alpha})\}$, bases of functions; namely,

$$F_{nlm}(\mathbf{y}, b) = (-1)^n N_{nl}\frac{1}{b^{3/2}} r^l L_n^{l+1/2}\left(r^2\right) \times$$
$$\times \exp\left\{-\frac{r^2}{2}\right\} Y_{lm}(\hat{\mathbf{y}}), \tag{6}$$

where

$$r = \frac{y}{b}, \quad N_{lm} = \sqrt{\frac{2\Gamma(n+1)}{\Gamma(n+l+3/2)}},$$

and

$$G_{\lambda\mu}(\mathbf{x}, b_\nu) = \frac{1}{b_\nu^{3/2}}\sqrt{\frac{2}{\Gamma(\lambda+3/2)}} \times$$
$$\times r^\lambda \exp\left\{-\frac{1}{2}r^2\right\} Y_{\lambda\mu}(\hat{\mathbf{x}}), \tag{7}$$

where $r = \frac{x}{b_\nu}$, respectively,

The total wave function of the nucleus is represented as the series expansion

$$\Psi^J = \sum_\alpha \sum_{\lambda_\alpha l_\alpha} \sum_{\nu_\alpha n_\alpha} C^{(\alpha)}_{\nu_\alpha \lambda_\alpha n_\alpha l_\alpha} \times$$
$$\times \hat{A}\left\{\left[\Phi_1(A_1)\,\Phi_2(A_2)\,\Phi_3(A_3)\right]_S \times \right.$$
$$\left. \times\left[G_{\lambda_\alpha}(\mathbf{x}_\alpha, b_{\nu_\alpha})\,F_{n_\alpha l_\alpha}(\mathbf{y}_\alpha, b)_L\right]\right\}_J, \tag{8}$$

where the expansion coefficients $\{C^{(\alpha)}_{\nu_\alpha \lambda_\alpha n_\alpha l_\alpha}\}$ with the fixed α-value ($\alpha = 1, 2, 3$) are nothing else than the Faddeev components in the discrete representation, three sets of which determine Ψ^J unambiguously.

In order to consider the bound and pseudobound states in two-cluster subsystems, the functions

$$|\nu, \alpha\rangle = \hat{A}\left\{\Phi_\beta(A_\beta)\,\Phi_\gamma(A_\gamma)\,G(\mathbf{x}_\alpha, b_\nu)\right\} \tag{9}$$

are constructed. By calculating the matrix elements of the two-cluster Hamiltonian using those functions, it is rather easy to obtain $E_\sigma^{(\alpha)}$, the binding energies of the ground ($\sigma = 0$) and excited (pseudobound, $\sigma > 0$) states, as well as the corresponding eigenfunctions $\{U_\nu^{(\sigma,\alpha)}\}$. The procedure is reduced to the solution of a relatively simple generalized problem of eigenvalues and eigenvectors,

$$\sum_{\tilde{\nu}}^{\langle\nu,\alpha|} H_\alpha^{(2)} - E_\sigma^\alpha\,|\tilde{\nu}, \alpha\rangle\,U_{\tilde{\nu}}^{(\sigma,\alpha)} = 0. \tag{10}$$

In order to solve the equations for the total wave function $\{C^{(\alpha)}_{\nu_\alpha\lambda_\alpha n_\alpha l\alpha}\}$ in the discrete representation, it is necessary to set the corresponding boundary conditions. In this work, only binary channels are considered. Therefore, only two-cluster asymptotics in the boundary conditions are discussed. In this case, $x_\alpha \ll y_\alpha$, i.e. the third cluster is located sufficiently far from the other two, which compose a bound subsystem. Let us denote the intercluster wave function for the bound state σ as $\phi^{(\alpha)}_{\sigma\lambda_\alpha}(x_\alpha)$. Then, for large magnitudes y_α of the Jacobi vector, the function $f^{(\lambda_\alpha,l_\alpha:L)}_{\alpha}(\mathbf{x}_\alpha,\mathbf{y}_\alpha)$ is factorized in the asymptotic region and takes the form

$$f^{(\lambda_\alpha\, l_\alpha\, L)}_{\alpha}(x_\alpha,y_\alpha)\approx\phi^{\alpha}_{\sigma\,\lambda_\alpha}(x_\alpha)\times \\ \times\left[S_{c_0,c_\alpha}\psi^{(-)}_{l_\alpha}(p_\alpha y_\alpha)-S_{c_0,c_\alpha}\psi^{(+)}_{l_\alpha}(p_\alpha y_\alpha)\right] \tag{11}$$

for the states in the continuous spectrum and

$$f^{(\lambda_\alpha\, l_\alpha\, L)}_{\alpha}(x_\alpha,y_\alpha)\approx-\phi^{\alpha}_{\sigma\,\lambda_\alpha}(x_\alpha)\times \\ \times\left[S_{c_0,c_\alpha}\Psi^{(+)}_{l_\alpha}(-i\,|p_\alpha|\,y_\alpha)\right] \tag{12}$$

for the bound states. Here, $\{c_\alpha\}$ is the set of all quantum numbers $(\lambda_\alpha, l_\alpha, ...)$ required to characterize a specific channel, and the subscript c_0 specifies the input channel. The momentum p_α is determined by the following relation:

$$p_\alpha=\sqrt{\frac{2m}{\hbar^2}\left(E-E^{(\alpha)}_{\sigma}\right)}. \tag{13}$$

Here, the state energy $E^{(\alpha)}_{\sigma}$ determines the threshold energy for the c_α-th channel in the two-cluster subsystem.

The factorization of the wave function $\{C_{\nu_\alpha\lambda_\alpha n_\alpha l_\alpha}\}$ also takes place in the discrete representation. The asymptotics is achieved at large n_α-values:

$$C^{(\alpha)}_{\nu_\alpha\lambda_\alpha n_\alpha l_\alpha}\approx U^{(\sigma,\alpha)}_{\nu_\alpha\lambda_\alpha}C^{(\alpha)}_{n_\alpha l\ \alpha}=U^{(\sigma,\alpha)}_{\nu_\alpha\lambda_\alpha}\sqrt{2r_{n_\alpha}}\times \\ \times\left[S_{c_0c_\alpha}\psi^{(-)}_{l_\alpha}(p_\alpha r_{n_\alpha})-S_{c_0c_\alpha}\psi^{(+)}_{l_\alpha}(p_\alpha r_{\ n_\alpha})\right], \\ C^{(\alpha)}_{\nu_\alpha n_\alpha}\approx U^{(\sigma,\alpha)}_{\nu_\alpha\lambda_\alpha}C^{(c_\alpha)}_{n_\alpha l_\alpha}=-U^{(\sigma,\alpha)}_{\nu_\alpha\lambda_\alpha}\sqrt{2r_{n_\alpha}}\times \\ \times\left[S_{c_0,c_\alpha}\psi^{(+)}_{l_\alpha}(-i\,|p_\alpha|\,r_{n_\alpha})\right], \tag{14}$$

where

$$r_{n_\alpha}=b\sqrt{4n_\alpha+2l_\alpha+3},$$

b is the oscillatory radius, and $\psi^{(-)}_{l_\alpha}(p_\alpha r_{n_\alpha})$ and $\psi^{(+)}_{l_\varepsilon}(p_\alpha r_{n_\alpha})$ are the radial asymptotic wave functions. The normalization is carried out per unit flow. The expansion coefficients $U^{(\sigma,\alpha)}_{\nu_\alpha\lambda_\alpha}$ represent the solution for the two-cluster Hamiltonian with a given number of Gaussian functions. Therefore,

$$\sum_{\nu_\alpha=1}^{N_\nu}U^{(\sigma,\alpha)}_{\nu_\alpha\lambda_\alpha}G_{\lambda_\alpha}(x_\alpha,b_{\nu_\alpha})=\phi^{(\alpha)}_{\sigma\lambda\ \alpha}(x_\alpha). \tag{15}$$

Formally, we have now to solve the infinite system of algebraic equations,

$$\sum_{c_\alpha}\sum_{\tilde{n}_{\tilde{\alpha}}}\left\langle\sigma,\lambda_\alpha;n_\alpha,l_\alpha;\alpha\middle|\hat{H}-E\middle|\tilde{\sigma},\tilde{\lambda}_{\tilde{\alpha}};\tilde{n}_{\tilde{\alpha}}\tilde{l}_{\tilde{\alpha}};\tilde{\alpha}\right\rangle C^{(c_{\tilde{\alpha}})}_{\tilde{n}_{\tilde{\alpha}}}=0. \tag{16}$$

In the same way as was done in the coordinate representation, it has to be supplemented with boundary conditions, in particular, at the matching point separating the inner and asymptotic regions for the wave function in the discrete space. For example, for the states of continuous spectrum, the expansion coefficients can be written as follows:

$$\left\{C^{(c_\alpha)}_{n_\alpha}\right\}=\left\{C^{(c_0)}_{0},C^{(c_1)}_{1},...,C^{(c_\alpha)}_{N_i},\sqrt{2r_{n_\alpha}}\times\right. \\ \left.\times\left[S_{c_0,c_\alpha}\psi^{(-)}_{l_\alpha}(p_\alpha r_{\tilde{n}_\alpha})-S_{c_0,c_\alpha}\psi^{(+)}_{l_\alpha}(p_\alpha r_{\tilde{n}_\alpha})\right]\right\}. \tag{17}$$

As a result, if N_c binary channels are considered, we obtain $N_cN_i + N_cN_c$ equations for determining N_cN_i coefficients of the wave function expansion in the inner region and N_cN_c equations for determining the elements of the S-matrix. The solution of this system of equations at a given potential makes it possible to obtain all necessary information about the bound states of the compound system and about the elastic scattering and reactions for a given energy value in the input channel.

The AMGOB was formulated in work [16]. It was used to describe the properties of states in the discrete and continuous spectra of p-shell nuclei [17–19].

3. Input Parameters of the Models and Calculation Results

Since the examined models are microscopic, the main input parameters for them are potentials specifying the interaction of the particles composing the system. To describe the central part of nucleon-nucleon interaction, the semiphenomenological modified Hasegawa–Nagata (MHN) potential was used,

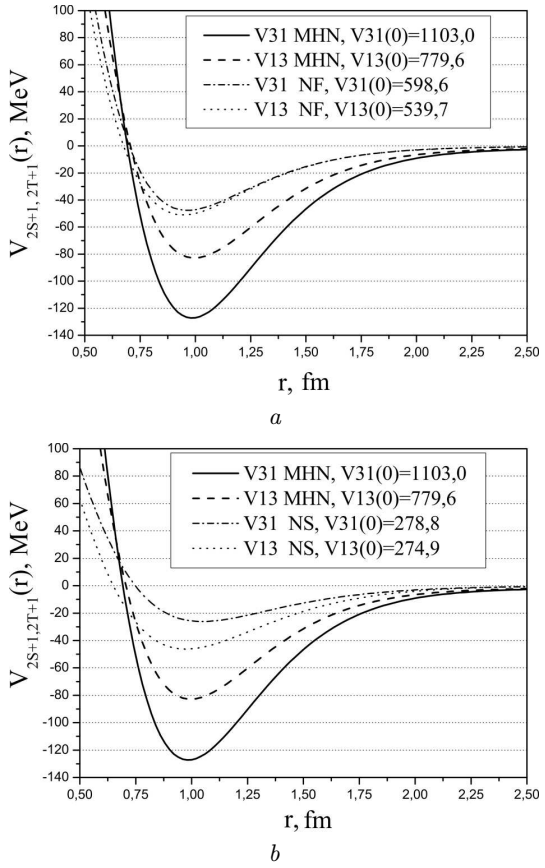

Fig. 1. Even components of the MHN potential and the YNG-NF (*a*) and YNG-NS (*b*) potentials

which is widely applied in the physics of light atomic nuclei [20]. For the interaction of nucleons with the Λ-hyperon, potentials from the YNG series [21] were used. This series includes the potentials YNG-ND, YNG-NF, YNG-NS, YNG-JA, and YNG-JB, which were obtained on the basis of the one-boson exchange concept. Here, the abbreviation YNG means that this is a hyperon(Y)-nucleon(N) potential given as a superposition of Gaussian (G) functions, and the letter N or J after the dash in the name means that the potential was obtained on the basis of the results obtained by the Nijmegen or Jülich group, respectively.

Running a little ahead, we note that, in the course of calculations, it was found that the application of the YNG-ND, YNG-JA, and YNG-JB potentials led to the inversion of the 0^+ and 1^+ levels in ${}^{4}_{\Lambda}$H, whereas the application of the YNG-NS potential resulted in a too large spin-spin splitting of those levels. Therefore, in what follows, the YNG-NF potential will be used, and we will only briefly dwell on its comparison with the YNG-NS potential.

Note right here that the components of the potentials belonging to the YNG series contain the Fermi wavenumber $k_{\rm F}$, which was immediately converted in practical calculations into the variational parameter. Therefore, below, we will consider it as a certain $k_{\rm eff}$. We point out that, in the calculations for ${}^{4}_{\Lambda}$H, which were carried out in the two-cluster version of the generator coordinate method with regard for the ${}^3{\rm H} + \Lambda$ clustering, the authors of the YNG potentials used the value $k_{\rm eff} = 0.80$ fm^{-1}. Again, since our models are three-cluster, there appears one more variation parameter, the oscillator radius b, which determines, in particular, the size of a deuteron cluster.

It is of interest to compare the behavior of the components of the NN and ΛN potentials as the functions of the interparticle distance and compare the NS and NF potentials for the ΛN potentials. For even components, which are mainly responsible for the attraction, this is done in Fig. 1 for the value $k_{\rm eff} = 0.84$ fm^{-1}. Despite that our NN and ΛN potentials are built in the framework of different approaches discussed above, we obtain a quite adequate picture from the viewpoint of meson exchange concepts. Nucleon-nucleon forces are more extended and intensive. Such a behavior can be associated with the fact that, unlike the NN interaction, bosons with the isospin equal to unity cannot participate in one-boson exchange in the case of ΛN forces because of the isospin prohibition. This also concerns π-mesons, which are the lightest ones. The same situation takes place for ρ-mesons, the exchange of which plays a substantial role in the formation of spin-orbit interaction.

When comparing the even components of ΛN potentials, it is easy to see that the difference between the spin-triplet and spin-singlet components of the NS potential is much larger than in the case of NF potential, which should be decisive for the spin-spin splitting of the 0^+ and 1^+ states.

3.1. Results of AMOB calculations

AMOB calculations were carried out for only one type of clustering, $({\rm D} + {\rm n}) + \Lambda$. The corresponding results will be considered proceeding from the comparison of the binding energies in the 0^+ and 1^+ states obtained using the NF and NS potentials (see Table 1).

Here, we draw attention to the fact that the energy splitting in the 0^+ and 1^+ states equals 0.77 MeV for the NF potential and -2.19 MeV for the NS one. In the former case, the splitting value may be somewhat underestimated in relation to the experiment, but it is drastically overestimated in the latter case. As a result, the 1^+ state can turn out higher than the lowest ${}^3\mathrm{H} + \Lambda$ threshold, which contradicts the experiment. By fixing, here and everywhere below, the parameters of the NN potential, i.e. taking the MHN potential in its original form, it is of interest to see how our results depend on the choice of k_{eff}. For this purpose, we calculated the binding energies and the root-mean-square radii for the bound states with k_{eff} varying from 0.70 to 0.90 fm^{-1}. The corresponding results are shown in Figs, 2 and 3.

As k_{eff} decreases, the state binding energies grow rather rapidly on the energy scale of the problem, and the values of the root-mean-square radii decrease, respectively. At the same time, the distance between the levels changes by about 0.1 MeV within the entire k_{eff}-interval. Thus, by choosing the value of k_{eff} within reasonable limits, we cannot radically affect the mutual arrangement of the $J^\pi = 0^+$ and $J^\pi = 1^+$ levels, if the YNG-NF potential is used, because the spin-singlet and spin-triplet components of the potential seem to change in a somewhat consistent way, when k_{eff} changes.

In order to get an idea of the mutual arrangement of clusters in the system, let us consider the correlation function. It is usually defined as the quantity $r_1 r_2 \left|\Psi_r\left(E_r, r_1, r_2\right)\right|^2$, where r_i is related to the Jacobi coordinates via the formula $r_i = q_i/\sqrt{\mu_i}$, and μ_i is the reduced mass. The sense of the correlation function consists in that it establishes a correspondence between the r_1- and r_2-values. In our case, those quantities mean the distance between the Λ-particle and the center of mass of the D + n subsystem and between the D and n clusters, respectively.

The correlation functions for the states 0^+ and 1^+ are shown in Fig. 4. The both plots are elongated along the r_1-axis, which is associated with the softness of the ${}^3\mathrm{H} + \Lambda$ cluster mode, which s caused, in turn, by the relative weakness of the ΛN interaction. But it should be marked right now that the wave functions of the system in both states include the functions of the main shell ($N = 0$) with very large weights. Their shares amount to about 85% and 81% for the ground and excited states, respectively. In addition, as one can see from the comparison of the panels, the correlation function for the 1^+ state is appreciably more elongated along r_1 than that for the

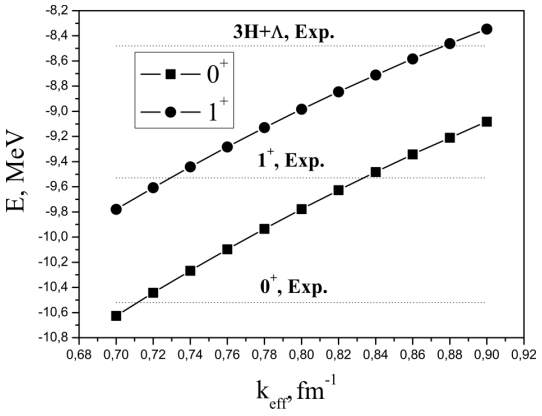

Fig. 2. Dependences of the energies of the $J^\pi = 0^+$ and $J^\pi = 1^+$ levels on the k_{eff}-value

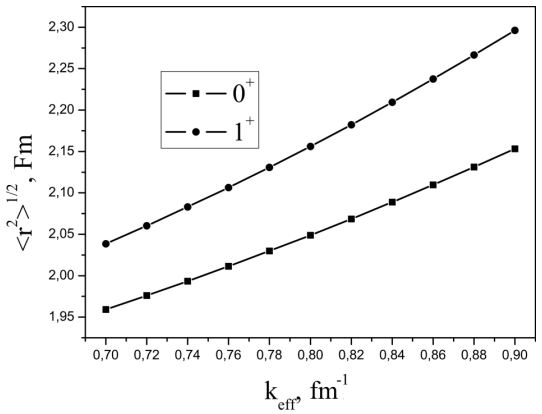

Fig. 3. Dependences of the root-mean-square radius on the k_{eff}-value for the $J^\pi = 0^+$ and $J^\pi = 1^+$ states

Table 1. **Energy (in MeV) and root-mean-square radius (in fm) of the ${}^{4}_{\Lambda}$H hypernucleus for the YNG-NF and YNG-NS potentials. $k_{\text{eff}} = 0.84$ fm^{-1}**

Modified Hasegawa–Nagata potential							
YNG-NF potential				YNG-NS potential			
$J^\pi = 0^+$		$J^\pi = 1^+$		$J^\pi = 0^+$		$J^\pi = 1^+$	
E	$\langle r^2\rangle^{1/2}$	E	$\langle r^2\rangle^{1/2}$	E	$\langle r^2\rangle^{1/2}$	E	$\langle r^2\rangle^{1/2}$
–9.482	2.089	–8.711	2.209	–9.992	2.036	–7.800	2.468

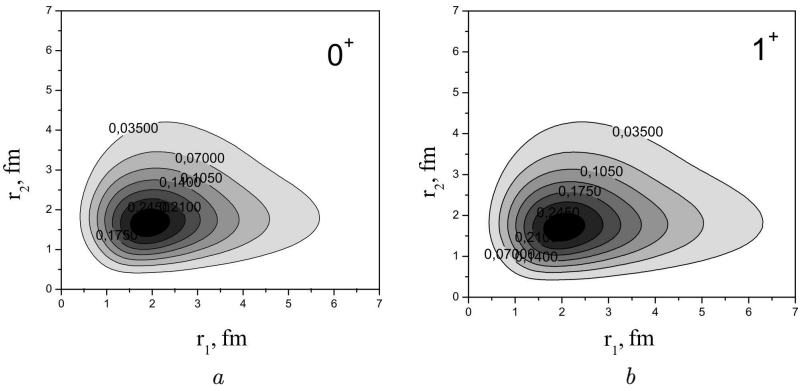

Fig. 4. Correlation functions for the $J^\pi = 0^+$ (a) and $J^\pi = 1^+$ (b) states

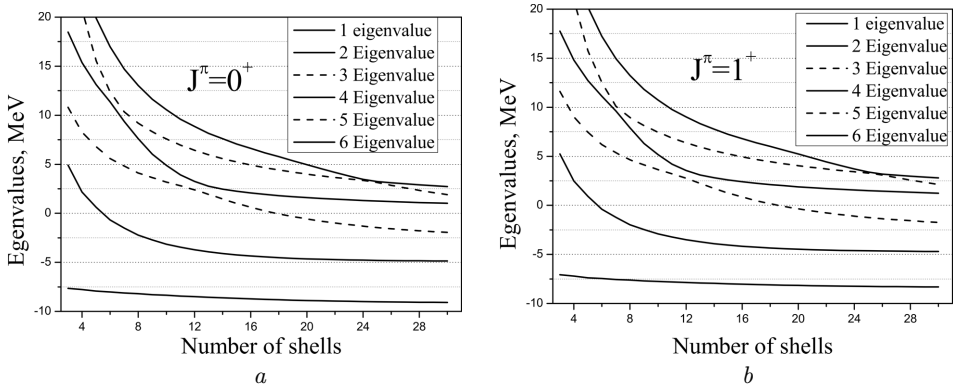

Fig. 5. Convergence of Hamiltonian eigenvalues for the $J^\pi = 0^+$ (a) and $J^\pi = 1^+$ (b) states

0^+ state. This means that, most likely, the state 1^+ is an excitation in the $^3\mathrm{H} + \Lambda$ channel.

In order to illustrate the convergence of the results as the function basis is expanded, Fig. 5 is presented. It demonstrates the dependences of the Hamiltonian eigenvalues on the number of the shell involved in calculations. These are all even shells with the principal quantum numbers $N = 0, 2, 4, ..., 60$. In addition to the good convergence, we should mark a characteristic behavior of eigenvalues: the eigenvalues descending from above "replace" those that reached a "plateau". This is a characteristic attribute that, in our model, resonances can occur in the three-cluster channel.

3.2. Results of AMGOB calculations

As was mentioned above, the AMGOB can be used to consider both the discrete and continuous spectral states making allowance for one or more binary channels and with the possibility to comsider the polarization of binary subsystems. First, let us dwell on the bound states, which have already been discussed in the previous section. Here, their binding energies will be temporally reckoned from the lowest decay threshold.

Figure 6 demonstrates the k_{eff}-dependences of the binding energies in the states 0^+ and 1^+. This figure completely reproduces (qualitatively) Fig. 2, and both those figures point out that if $k_{\mathrm{eff}} = 0.84$ fm^{-1}, we obtain an almost exact position of the ground state with respect to the lowest threshold of the $^3\mathrm{H} + \Lambda$ decay.

Accordingly, we can try to consider the scattering of the Λ particle by ^{3}H. Figure 7 shows the energy dependence of the scattering phases of the Λ-hyperon by ^{3}H with regard for various polarization degrees of the latter, which is considered as the binary subsystem D + n. Here, in accordance with the notation introduced in Section 2.2, N_G is the number of Gaussian functions involved in calculations, and $\lambda_{\max}$ is the maximum partial momentum.

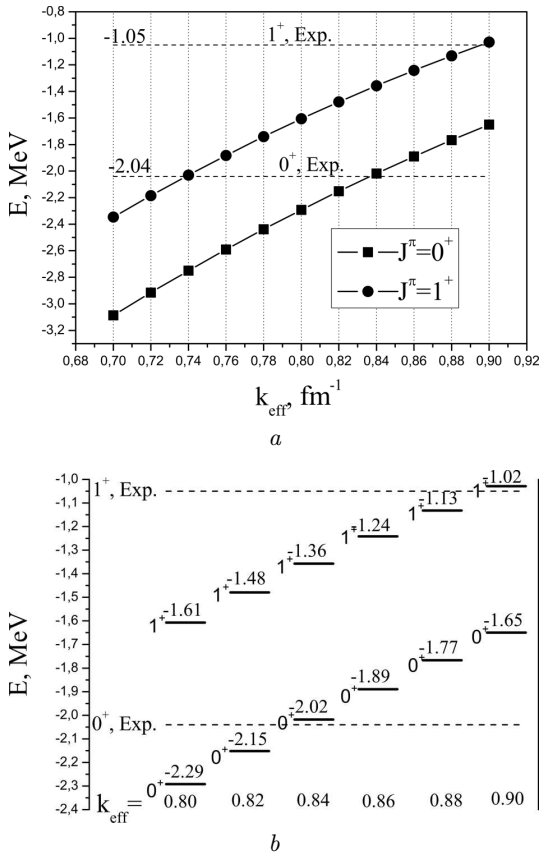

Fig. 6. Dependences of the energies of the levels $J^\pi = 0^+$ and $J^\pi = 1^+$ on the k_{eff}-value. The energies are reckoned from the ${}^3\text{H} + \Lambda$ decay threshold

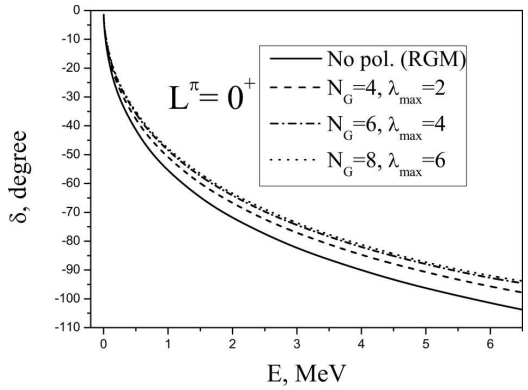

Fig. 7. Influence of the ${}^3\text{H}$ polarization on the scattering phases for ${}^3\text{H} + \Lambda$ with $L^\pi = 0^+$

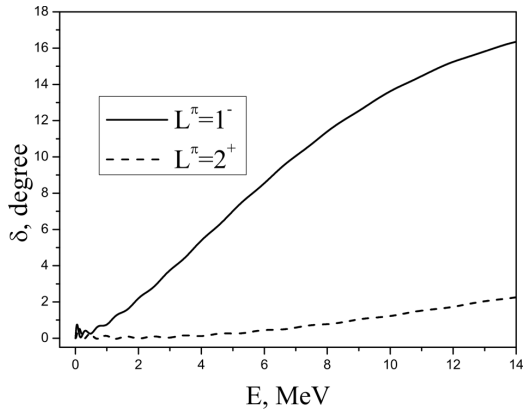

Fig. 8. Scattering phases for ${}^3\text{H} + \Lambda$ with $L^\pi = 1^-$ and 2^+

From Fig. 7, one can see that the account for the possible polarization of the binary subsystem appreciably changes the scattering phases and leads to the growth of the attraction between ${}^3\text{H}$ and Λ. At the same time, Fig. 8, despite that the scattering phases were not calculated quite accurately at low energies, testifies that there are no kinematic resonances with any reasonable widths in the states with $L = 1^-$ and 2^+.

Unfortunately, we cannot compare the last results with experimental or other theoretical data, because such data are absent. Therefore, let us return to the calculation results obtained for the bound states in the AMGOB, where such a comparison can be done.

In Table 2, the results of calculations of the binding energy in the 0^+ and 1^+ states in three versions of the AMGOB are quoted. Version 1 corresponds to the complete calculation in the framework of the AM-

Table 2. **Calculation versions of the energy (in MeV) of the states $J^\pi = 0^+$ and $J^\pi = 1^+$ of the ${}^4_{\Lambda}\text{H}$ hypernucleus for various k_{eff}-values from 0.8 to 0.9 fm^{-1}. The obtained energy for the ${}^3\text{H}$ nucleus equals −7.01 MeV. See other explanations in the text**

k_{eff}	0.80	0.82	0.84	0.86	0.88	0.90
			$J^\pi = 0^+$			
1	–9.296	–9.156	–9.022	–8.894	–8.771	–8.654
2	–9.261	–9.121	–8.988	–8.860	–8.738	–8.621
3	–6.744	–6.521	–6.304	–6.090	–5.882	–5.678
			$J^\pi = 1^+$			
1	–8.611	–8.483	–8.361	–8.246	–8.136	–8.033
2	–8.587	–8.460	–8.338	–8.223	–8.114	–8.013
3	–5.753	–5.528	–5.308	–5.092	–4.880	–4.674

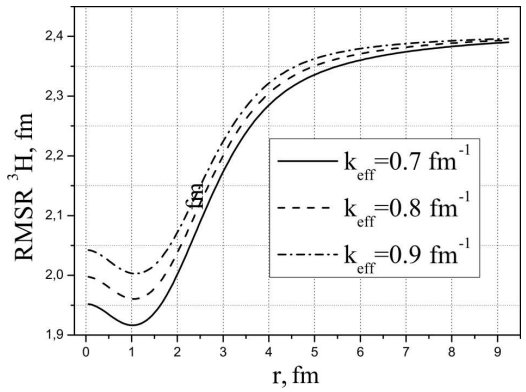

Fig. 9. Dependences of the root-mean-square radius of ^{3}H on the distance between the center of mass of ^{3}H and the Λ-particle for various k_{eff}-values

GOB. In other words, all clustering types–(D + n) + +Λ, (D + Λ) + n, and D + (n + Λ)–are taken into account simultaneously, and the polarization of binary subsystems is made allowance for. In version 2, only one type of clustering – namely, (D + n) + Λ with the polarization of the (D + n) subsystem – is taken into consideration. Version 3 differs from version 1 in that the possibility of the polarization of binary subsystems is not taken into account.

Comparing the results of calculations in versions 1 and 2, we note that the energies of the states $J^\pi = 0^+$ and $J^\pi = 1^+$ are practically identical for them. This means that the dominant role in the formation of those states is played by the cluster structure (D + + n) + Λ. Accordingly, the results obtained in the AMOB in Section 3.1 can be considered as qualitatively reasonable. The calculation results obtained for version 3 testify to the importance of a good description of binary subsystems, in particular, as we now understand, the subsystem (D + n).

From the aforesaid, it follows that we almost nothing lose in the calculation accuracy for the binding energies in the bound states, if we involve only one type of clustering, (D + n) + Λ, in calculations and try to reproduce the binding energy for ^{3}H = D + n. Here, we will try to describe the relative motion of clusters D and n as accurately as possible and apply the variation of the oscillatory radius b. The value of the latter was 1.67 fm in previous calculations, which allowed the energy of the lowest decay threshold to be reproduced easily. However, in order to improve the description of the binding energy in ^{3}H, the value $b = 1.50$ fm was required. As a result, this made it possible to increase the ^{3}H binding energy from 7.01 to 7.74 MeV.

The final results of calculations for the binding energies in the bound states are presented in the next subsection, where we compare them with the results of other authors. Here, in Fig. 9, we depict a plot illustrating the dependence of the root-mean-square radius of the ^{3}H = D + n subsystem as a function of the distance from the center of mass of this subsystem to the Λ-particle for various k_{eff}-values. One can see that in spite of the fact that the ΛN interaction is weaker than the NN one, the Λ-hyperon can polarize ^{3}H rather strongly.

Table 3. **Energies of the 0^+ and 1^+ states obtained in work [22] in the four-cluster model using the NN potential AV8 and the ΛN potential NSC97f and considering all possible Jacobi trees, as well as our results obtained for only one type of clustering, (D + n) + Λ. $E(^3H) = -7.77$ MeV in work [22] and −7.74 MeV in our case**

State	Results of work [22]	Our results		Experiment
		AMOB	AMGOB	
0^+	–10.10	–10.12	–10.04	–10.52
1^+	–8.36	–9.30	–9.24	–9.53

3.3. Comparison with experimental and other theoretical results

While comparing our results with the results of other authors, we start from work [22], where, according to the cited authors, the main purposes were as follows: firstly, to solve the four-particle problem for the $^4_\Lambda$H hypernucleus making allowance for the NNNΛ(Σ) channels and using realistic NN and YN interactions and, secondly, to clarify the role of the ΛN-ΣN bond in hypernuclei with $A = 4$. The calculations were carried out in the framework of the variational method and applying the Gaussian functions of the Jacobi coordinates. As the NN potential, the AV8 potential was mainly used. At the same time, the ΛN interaction was simulated by means of the NSC97f potential, which, according to the statement of cited authors, is the only workable potential from the NSC97a-f series. The results obtained in work [22] for the total binding energies are quoted in Table 3 together with our results and relevant experimental data.

Our binding energy values for ^{3}H are close to those obtained in work [22]. This is also true for the ground-state energies. At the same time, the energies are rather different for the 1^+ state. Most likely, it occurs due to the fact that the strongly overestimated spin-spin splitting is incorporated into the NS potentials from the very beginning.

For comparison, we also present the results of work [23], which were obtained using the No-Core Shell Model (NCSM). The NCSM essence consists in the expansion of the multiparticle wave function of the nucleus in an as large as possible basis of the shell model functions. According to the cited authors, this procedure, together with the inclusion of the potentials that were obtained using the chiral perturbation theory, allowed them to say that their calculations were carried out on the basis of first principles (*ab initio*).

Because of the poor convergence of the results, which the authors of work [23] explained by a high looseness of the hypernucleus, they extrapolated their results to the case where the maximum value of the principal oscillator number tends to infinity. The corresponding results are shown in Table 4.

Note that the authors of work [23] obtained the values that are almost equal to the experimental value of the binding energy for ^{3}H. But this fact does not mean that the chiral perturbation theory provides potentials that allow obtaining exact values for the binding energy in three-nucleon systems. It occurred because in work [24], the potential parameters, which were obtained using the chiral perturbation theory, were specified exactly using three-particle experimental data.

For a comparison of our results with theoretical results of other authors and experimental data to be more illustrative, we present a plot in Fig. 10, where the binding energies are reckoned from the ^{3}H + Λ decay thresholds. The comparison of our results with experimental data, as well as with the results of the most consistent theoretical works, demonstrates that, currently, it is not yet possible to describe the relatively simple spectrum of the bound states of the ${}^{4}_{\Lambda}$H hypernucleus at length. The main difficulty is connected with the uncertainty of interaction potentials between the particles, first of all, the ΛN potential. At the same time, the results of our calculations do not fall out of a number of calculation results obtained in the framework of the models that are currently the most accurate. Furthermore, they allow pointing out some features of the ${}^{4}_{\Lambda}$H structure.

Table 4. **Extrapolated values of the ground and first excited state energies for various values of the Λ interaction regulator [23]. The ^{3}H energy obtained using the NN potential [24] equals −8.47 MeV**

State	Λ, MeV/s			
	550	600	650	700
0^+	–11.20(6)	–10.95(4)	–10.83(5)	–10.85(3)
1^+	–10.29(25)	–9.87(28)	–9.55(35)	–9.20(30)

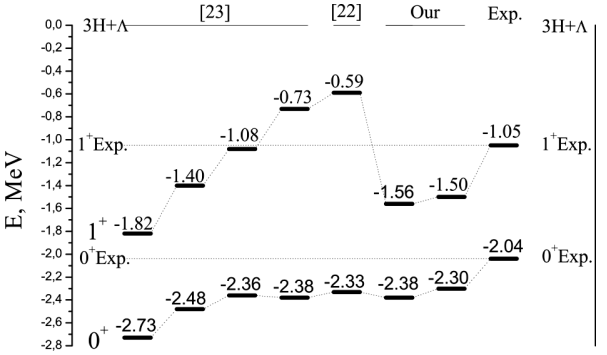

Fig. 10. Comparison of our results with the theoretical results of other authors and experimental data. The energy is measured from the ^{3}H + Λ decay thresholds

4. Conclusions

The properties of the states of the ${}^{4}_{\Lambda}$H hypernucleus have been considered in the framework of two three-cluster models: the AMOB, where only the cluster representation (D + n) + Λ was used, and the AMGOB, where all possible clustering types, i.e. (D + n) + Λ, (D + Λ) + n, and D + (n + Λ), were taken into account in calculations. The calculations in the framework of the latter model showed that the cluster representation (D + n) + Λ with making allowance for the polarization undoubtedly plays a dominant role in the proper description of the ${}^{4}_{\Lambda}$H hypernucleus properties. An important factor at that is a necessity of the best description for the binary subsystem D + n. The results obtained in the framework of the AMOB also completely satisfy those criteria. A

comparison of our results with the results obtained in the most consistent models showed that our results fall quite well into the body of relevant data.

This work was partially sponsored by the National Academy of Sciences of Ukraine (project No. 0117U000239).

1. E. Hiyama, T. Yamada. Structure of light hypernuclei. *Prog. Part. Nucl. Phys.* **63**, 339 (2009).
2. Y. Kanada-En'yo. Excitation energy shift and size difference of low energy levels in *p*-shell Λ hypernuclei. *Phys. Rev. C* **97**, 024330 (2018).
3. Y. Kanada-En'yo. Structures of p-shell double Λ-hypernuclei studied with microscopic cluster models. *Phys. Rev. C* **97**, 034324 (2018).
4. L.L. Margolin. Microscopic investigation of the structure characteristics and wave functions of the five-body hypernucleus. *Eur. Phys. J. Web Conf.* **66**, Di (2014).
5. E. Hiyama, Y. Yamamoto, T. Motoba, M. Kamimura. Structure of $A = 7$ iso-triplet Λ-hypernuclei studied with the four-body cluster model. *Phys. Rev. C* **80**, 054321 (2009).
6. A. Feliciello, T. Nagae. Experimental review of hypernuclear physics: recent achievements and future perspectives. *Rep. Prog. Phys.* **78**, 096301 (2015).
7. W.M. Alberico, G. Garbarino. Weak decay of Lambda hypernuclei. *Phys. Rept.* **369**, 1 (2002).
8. Q.N. Usmani, A.R. Bodmer, Z. Sauli. Core nucleus polarization in Λ hypernuclei. *Phys. Rev. C* **77**, 034312 (2008).
9. Th.A. Rijken, V.G.J. Stoks. Soft-core hyperon-nucleon potentials. *Phys. Rev. C* **59**, 21 (1999).
10. M.M. Nagels, Th.A. Rijken, Y. Yamamoto. Extended-soft-core baryon-baryon model ESC16. II. Hyperon-nucleon interactions. *Phys. Rev. C* **99**, 044003 (2019).
11. K. Wildermuth, Y.-C. Tang. *Unified Theory of the Nucleus* (Academic Press, 1977).
12. G.F. Filippov, I.P. Okhrimenko. On the possibility of using the oscillatory basis for solving continuous spectrum problems. *Yad.Fiz.* **32**, 932 (1980) (in Russian).
13. G.F. Filippov. On the account of correct asymptotics in the expansions in the oscillatory basis. *Yad. Fiz.* **33**, 928 (1981) (in Russian).
14. A.V. Nesterov, F. Arickx, J. Broeckhove, V. Vasilevsky. Three-cluster description of the properties of light neutron- and proton-rich nuclei in the framework of the algebraic version of the resonating group method. *Elem. Chast. At. Yadro* **41**, 1337 (2010) (in Russian).
15. V.S. Vasilevsky, A.V. Nesterov, F. Arickx, J. Broeckhove. Algebraic model for scattering in three-*s*-cluster systems. II. Resonances in three-cluster continuum of ^{6}He and ^{6}Be. *Phys. Rev. C* **63**, 034607 (2001).
16. V.S. Vasilevsky, F. Arickx, J. Broeckhove, T.P. Kovalenko. A microscopic three-cluster model with nuclear polarization applied to the resonances of ^{7}Be and the reaction ^{6}Li(p,^{3}He)^{4}He. *Nucl. Phys. A* **824**, 37 (2009).
17. A.V. Nesterov, V.S. Vasilevsky, T.P. Kovalenko. Influence of cluster polarization on the spectrum of the ^{7}Li nucleus and the ^{6}Li (n, ^{3}He)^{4}He reaction. *Yad. Fiz.* **72**, 1505 (2009) (in Russian).
18. Y.A. Lashko, G.F. Filippov, V.S. Vasilevsky. Microscopic three-cluster model of ^{10}Be. *Nucl. Phys. A* **958**, 78 (2017).
19. V.S. Vasilevsky, N. Takibayev, A.D. Duisenbay. Microscopic description of ^{8}Li and ^{8}B nuclei within a three-cluster model. *Ukr. J. Phys.* **62**, 461 (2017).
20. A. Hasegawa, S. Nagata. Ground state of ^{6}Li. *Prog. Theor. Phys.* **45**, 1786 (1971).
21. Y. Yamamoto, T. Motoba, H. Himeno, K. Ikeda, S. Nagata. Hyperon-nucleon and hyperon-hyperon interactions in nuclei. *Prog. Theor. Phys. Suppl.* No. 177, 361 (1994).
22. E. Hiyama, M. Kamimura, T. Motoba, T. Yamada, Y. Yamamoto. Λ-Σ conversion in and based on a four-body calculation. *Phys. Rev C* **65**, R011301 (2001).
23. R. Wirth, D. Gazda, P. Navratil, R. Roth. Hypernuclear no-core shell model. *Phys. Rev. C* **97**, 064315 (2018).
24. A.M. Shirokov, J.P. Vary, A.I. Mazur, T.A. Weber. Realistic nuclear Hamiltonian: Ab exitu approach. *Phys. Lett. B* **644**, 33 (2007).

Received 12.08.21

Translated from Russian by O.I. Voitenko

О.В. Нестеров, М. Солоха-Климчак

ВЛАСТИВОСТІ ГІПЕРЯДРА $^4_\Lambda$H
У ТРИКЛАСТЕРНИХ МІКРОСКОПІЧНИХ МОДЕЛЯХ

В рамках мікроскопічних трикластерних алгебраїчних моделей з можливим урахуванням типів кластеризації (D + + n) + Λ, (D + Λ) + n, та (n + Λ) + D розглянуто властивості станів дискретного спектра гіперядра $^4_\Lambda$H і станів неперервного спектра в каналі ^{3}H + Λ. Продемонстровано, що кластерна структура $^4_\Lambda$H практично повністю визначається кластеризацією (D + n) + Λ при цілком відчутному впливі поляризації бінарної підсистеми (D + n) за рахунок взаємодії з Λ-частинкою.

Ключові слова: кластерні моделі, метод резонуючих груп, трикластерні мікроскопічні моделі, алгебраїчні моделі, гіперядера, кластерна поляризація.